# Simultaneous catalyzing and reinforcing effects of imidazole-functionalized graphene in anhydride-cured epoxies

Liu, Wanshuang; Koh, Kwang Liang; Lu, Jinlin; Yang, Liping; Phua, Si Lei; Kong, Junhua; Chen, Zhong; Lu, Xuehong

2012

Liu, W., Koh, K. L., Lu, J., Yang, L., Phua, S., Kong, J., et al. (2012). Simultaneous catalyzing and reinforcing effects of imidazole-functionalized graphene in anhydride-cured epoxies. Journal of Materials Chemistry, 22(35), 18395-18402.

https://hdl.handle.net/10356/96645

https://doi.org/10.1039/C2JM32708B

| | |
|---|---|
| Title | Simultaneous catalyzing and reinforcing effects of imidazole-functionalized graphene in anhydride-cured epoxies |
| Author(s) | Wanshuang Liu, Kwang Liang Koh, Jinlin Lu, Liping Yang, Silei Phua, JunhuaKong, Zhong Chen and Xuehong Lu |
| Citation | |
| Date | 2012 |
| URL | http://hdl.handle.net/null |
| Rights | |

Journal Name

Dynamic Article Links ►

Cite this: DOI: 10.1039/c0xx00000x

www.rsc.org/xxxxxx

ARTICLE TYPE

# Simultaneous catalyzing and reinforcing effects of imidazole-functionalized graphene in anhydride-cured epoxies†

**Wanshuang Liu, Kwang Liang Koh, Jinlin Lu, Liping Yang, Silei Phua, Junhua Kong, Zhong Chen, Xuehong Lu***

In this study, imidazole-functionalized graphene (G-IMD) was prepared from graphene oxide by a facile one-pot method. The functionalized graphene not only showed improved organic compatibility but also could simultaneously play the roles as cure accelerator and reinforcement for anhydride-cured epoxies. Our results showed that G-IMD could successfully catalyze the curing reaction without adding any routine accelerator. Thermal and mechanical properties of the epoxy/G-IMD nanocomposites were systematically studied at different filler loadings. Compared with neat epoxy resin, tensile strength and Young's modulus of the nanocomposites were enhanced by 97% and 12%, respectively, at only 0.4 wt % G-IMD loading. Dynamic mechanical analysis and electron microscopic results revealed that the drastic improvements in mechanical properties could be attributed to the homogeneous dispersion of G-IMD and covalent bonding at interface, which effectively improved the efficiency of load transfer between the matrix and graphene.

## 1. Introduction

As a type of classic thermosetting polymers, epoxy resins are well-established matrix materials for high-performance composites used in a wide variety of industrial areas, such as wind energy, automotive and aerospace, owing to their excellent combination of good stiffness, dimensional stability, environmental resistance and strong adhesion to the embedded reinforcement. Nevertheless, an inherent limitation of epoxy resins is that their stiffness is highly dependent on crosslink density, whereas too high a crosslink density may result in brittle failure at a very low strain. To address this issue, vigorous efforts have been undertaken to enhance the ultimate strength and fracture toughness of epoxy resins without sacrificing their stiffness, among which an effective approach is to incorporate nano-sized reinforcements such as silica,[1] clay[2,3] and carbon.[4,5]

With respect to carbon-based nanofillers, graphene, an ideal one-atom-thick planar sheet of $sp^2$-bonded carbon atoms, has sparked intensive research interests in the past few years. Besides excellent electrical and thermal properties, graphene also holds great potential as a promising reinforcement for advanced composite materials.[6,7] Researchers at Columbia University have demonstrated that monolayer graphene is presently the strongest material ever measured with about 1 TPa in Young's modulus and 130 GPa in ultimate strength.[8] In addition, the large specific surface areas and wrinkled morphology of graphene sheets may help to build a strong interface, facilitating the stress transfer from polymer matrices to graphene.[5] However, just like the nanocomposites reinforced by other types of nanofillers, the macroscopic performance of a graphene-reinforced nanocomposite also depends heavily on the dispersion state of graphene sheets and the extent of interfacial interactions. Pristine graphene has a pronounced tendency to agglomerate in epoxy matrices owing to the poor compatibility between graphene and the resins as well as the strong Vander Waals force and π-π interactions between the graphene sheets.[9,10] Covalent incorporation of graphene into epoxy matrices can synchronously improve dispersibility and interfacial interactions.[11] Some amino- and epoxy-functionalized graphene have been proven to be effective reinforcements for epoxy resins as the functional groups actively participate in the curing process and thus integrate the epoxy networks and graphene sheets though strong covalent archoring.[12-15] For example, Kim et al. reported 4-aminobenzoyl-functionalized graphene-like platelets as a co-curing agent and nano-reinforcement for an epoxy resin. Their mechanical testing results revealed that average tensile strength and Young's modulus were increased by approximately 30% and 40%, respectively, at 4 wt % filler loading.[12]

So far the work on graphene-reinforced epoxy nanocomposites are mainly focused on traditional amine/epoxy systems, whereas the researches on anhydride/epoxy systems have hardly been reported. It is well known that anhydride-cured epoxy resins have some unique advantages including low viscosity, long working life and good thermal stability over amine-cured epoxy systems.[16,17] These advantages are highly desirable for fabrication of high-performance composites using processes such as filament winding and resin transfer moulding. Furthermore, the cure

profiles of anhydride/epoxy systems can be tailored via catalysts, such as imidazoles, to suit for different applications. In this work, aiming at reinforcing anhydride-cured epoxies with covalently bonded graphene, an imidazole-functionalized graphene (G-IMD) was prepared using a facile one-pot method starting from graphene oxide (GO). The effects of the functionalization on organic compatibility, catalytic and reinforcing effects of the graphene sheets were investigated, with the emphasis on the influences of the functionalization on thermal and mechanical properties of the nanocomposites.

## 2. Experimental

### 2.1 Materials

Natural graphite flake (43319, -10 mesh, 99.9%) and potassium permanganate were supplied by Alfa Aesar (USA). N,N-Dimethylformamide (ACS reagent, ≥99.8%), $H_2SO_4$ (95-97%), sodium nitrite, hydrochloric acid (37%), hydrogen peroxide (30%), sodium borohydride ($NaBH_4$, >98%), 1-(3-aminopropyl)imidazole, 2-ethyl-4-methylimidazole (EMI) and hexahydro-4-methylphthalic anhydride were purchased from Aldrich-Sigma Chemicals Inc. (USA) and used without further purification. Epoxy (DER 332) with epoxy equivalent weight of 171-175 was supplied by Dow Chemicals (USA).

### 2.2 Synthesis of GO, rGO and imidazole-functionalized graphene (G-IMD)

GO was prepared from the natural graphite by a modified Hummers method[18] and the details could be found in the Electronic Supplementary Information (ESI). In a typical reaction for preparing G-IMD, 400 mg GO was firstly dispersed into 200 mL of DI water using bath sonication for 2 h. The suspension was purified by three cycles of centrifugation at 4,000 rpm for 30 min, and a rather small quantity of precipitate was discarded to remove unexfoliated particles. The obtained supernatant and 4 g 1-(3-aminopropyl) imidazole (about 10 equiv/weight of GO) were added into a 500 ml flask purged with $N_2$. The mixture was heated at 70 °C with magnetic stirring for 36 h to obtain a homogeneous black dispersion. After cooling to room temperature, the pH of this solution was carefully adjusted to 9 - 10 using 5 wt % sodium carbonate solution. Subsequently, 1.13 g $NaBH_4$ (150 mM) was directly added into the mixture under magnetic stirring and $N_2$ atmosphere. The mixture was kept at 80 °C for 1 h with constant stirring. The product was separated by centrifugation at 11,000 rpm for 15 min followed by washing with large amounts of DI water. Five cycles of this purification were performed to remove the residual ions and excessive raw materials. The final product was freeze-dried for 48 h. GO was also reduced by $NaBH_4$ to produce reduced GO (rGO) as a reference material using the procedures similar to that for the reduction of G-IMD.

### 2.3 Preparation of epoxy/G-IMD composites

G-IMD was first dispersed in DMF (concentration: 0.5 mg $ml^{-1}$) with the assistance of ultrasonication for 30 min. Epoxy DER 332 and hexahydro-4-methylphthalic anhydride with a stoichiometric equivalent ratio (epoxy groups/anhydride groups = 1:1), were homogeneously mixed and then the mixture was added to the G-IMD suspension. After ultrasonication for another 30 min, the DMF was completely removed under reduced pressure (5-15 mbar) at 70 °C. Subsequently, the mixture was poured into a PTFE mold and degassed for 1 h at a vacuum approaching about 0.1 mbar. The nanocomposites were cured using the following profile: 140 °C for 2 h, 160 °C for 4 h and finally 180 °C for 2 h. Sample bars for tensile testing and dynamic mechanical analysis (DMA) were obtained by curing in the mold with specific dimensions. As a reference, pristine epoxy/anhydride mixture was cured under the same condition, except that 1.0 wt % EMI was added as catalyst.

### 2.4 Characterization

Fourier transform infrared (FTIR) spectra were obtained using a Perkin Elmer Instruments Spectrum GX FTIR spectrometer at room temperature with a wave number range from 600 to 4000 $cm^{-1}$. All of the samples were prepared as pellets using spectroscopic grade KBr. X-ray photoelectron spectroscopy (XPS) measurements were performed on a Kratos Analytical AXIS His spectrometer with a monochromatized Al Ka X-ray source (1486.6 eV photons). Elemental analysis was performed using Perkin Elmer Instruments CHNS-O Analyzer. The weight percentage (%) composition of Carbon, Hydrogen and Nitrogen were measured. Atomic force microscope (AFM) observation of G-IMD was conducted on a Dimension 3100 AFM (Digital Instruments). The samples were dispersed in DMF (~ 0.02 mg $ml^{-1}$) by ultrasonication and dip-coated onto fresh Si wafers cleaned with a piranha solution. Transmission electron microscopy (TEM) was performed on JEOL-2010 with accelerating voltage of 200 kV. For G-IMD, the sheets were first dispersed in DMF (~ 0.02 mg $ml^{-1}$) with ultrasonic, and then collected on 200 mesh copper grids. For epoxy/G-IMD nanocomposites, the samples were prepared by ultramicrotome with a thickness of 50-70 nm at room temperature in water. Wide angle X-ray scattering (WAXS) patterns were recorded in a Bruker D8 Advanced XRD using Cu Kα1 radiation. Differential scanning calorimetry (DSC) was recorded on a TA Instruments DSC 2920 using $N_2$ as a purge gas at a heating rate 3 °C $min^{-1}$. Thermal gravimetric analysis (TGA) were performed on a TA Instruments TGA Q 500 under a nitrogen atmosphere over a temperature range of 25 - 800 °C at a heating rate of 10 °C $min^{-1}$. The instruments and conditions for the dynamic mechanical analysis (DMA) were the same as those reported in our previous publication except the sample length was 40 mm.[19] Tensile tests were performed using an ITW Instron Tester 5567 with a 3,000 N load cell at a crosshead speed of 1 mm $min^{-1}$. The dog-bone shaped tensile samples were prepared according to the ASTM D638 standard and polished to 60 mm × 7 mm × 1.6 mm. Each reported value is the average of at least six specimens. The morphologies of the fracture surfaces of the tensile bars were investigated by JEOL FESEM 7600F field emission scanning electron microscope (FESEM). The sample was coated with gold for 100 sec.

## 3. Results and discussion

### 3.1 Synthesis, structure and morphology of G-IMD

It's well known that GO contains a large amount of reactive oxygen-containing groups such as hydroxyl, epoxy, carboxyl, and carbonyl, which opens up a versatile avenue for a variety of chemical transformations.[20] Among these reactive groups, epoxy

groups on the basal planes of GO can easily react with amines through ring-opening reaction under a mild condition.[21,22] In this study, we adopt a strategy of functionalization prior to reduction to prepare G-IMD. The synthesis route is illustrated in Scheme 1. Using this one-pot approach, 1-(3-aminopropyl) imidazole firstly reacts with GO and then the modified GO is reduced by $NaBH_4$. $NaBH_4$, instead of hydrazine hydrate, is herein chosen as the reducing agent because $NaBH_4$ can reduce GO more effectively,[23] whereas hydrazine derivative may be further grafted onto the functionalized graphene, producing byproducts.[21] Moreover, the synthesis condition is mild and the whole process is carried out in aqueous medium.

XPS and FTIR spectra are important tools for the characterization of chemically converted graphene. Fig. 1 shows the XPS spectra of GO, rGO and G-IMD. The high-resolution C1s XPS spectra of GO (Fig. 1a) shows four types of carbons: C-O-C (286.7 eV), C-OH (286.0 eV), C=O (287.7 eV), O=C-O (289.5 eV), which are in good agreement with previous reports.[21,24,25] After reduction, the C1s XPS spectra of rGO and G-IMD reveal that the peaks arising from oxygen-related groups significantly decrease in intensity. Compared with rGO, new peaks from C=N (285.5 eV) and C-N (286.5 eV)[25-27] appear in the C1s XPS spectra of G-IMD. Moreover, nitrogen-related bands arising from imidazole ring (401.3 eV and 398.9 eV) and amide (400.1 eV)[28-30] can be observed in deconvoluted N1s XPS spectra of G-IMD (Fig. 1b), confirming that 1-(3-aminopropyl)imidazole had been covalently bonded onto graphene via the amide linkage. The results of the FTIR spectra (Fig. 1c) are consistent with XPS data. The distinctive feature of GO spectrum lies in the characteristic carbonyl stretching band ν (C=O) at ca. 1740 $cm^{-1}$. The intensity of this peak drastically decreases in the spectra of rGO and G-IMD, suggesting that GO was effectively reduced by $NaBH_4$. In the FTIR spectrum of G-MD, new bands at 2925 and 2855 $cm^{-1}$ can be attributed to symmetric stretching band νs (C-H) and asymmetric stretching band νas (C-H) from alkyl groups, while the bands at 1505, 1110 and 815 $cm^{-1}$ can be attributed to imidazole ring vibration and deformation band δ (N-H) in amide.[31,32] In addition, the band at 1440 $cm^{-1}$ is most likely to be a combined band of imidazole ring vibration and deformation band δ (C-H).[32]

Additionally, WAXS and TGA studies also provide circumstantial evidence about the successful modification and reduction. WAXS studies show that the sharp X-ray diffraction peak of GO ($2\theta = 9.83°$)[33] nearly disappears in the patterns of rGO and G-IMD (Fig. S1 in the ESI†), indicating the effective reduction of GO by $NaBH_4$. TGA results (Fig. S2 in the ESI†) reveal that in a $N_2$ atmosphere, the difference in weight loss between rGO and G-IMD is about 20 wt % in the temperature range of 500 to 700 °C. rGO and G-IMD show weight losses of 19 and 38%, respectively, at 700 °C. Assuming the removal of the grafted amino imidazole has completed at 700 °C, the degree of functionalization is estimated to be ~1 functional group for every 26 carbons. Elemental analysis results (Table S1 in the ESI†) show that the nitrogen content in G-IMD is about 10.9 wt %. As all the nitrogen atoms should come from the amino imidazole, the weight percent of the grafted amino imidazole is estimated to be about 32%.

AFM was used to examine the dimensions of the G-IMD sheets dispersed in DMF. Figs. 2a and 2b reveal that the thickness of single-layer G-IMD varies from 1.0 to 1.4 nm according to cross-sectional analysis, which is slightly thicker than the reported individual graphene layer (0.6 - 0.9 nm).[34,35] The slightly larger height and bumpy surface are likely due to the grafted amino imidazole moieties and a small quantity of residue oxygen-containing groups on graphene surface. TEM provides further evidence for the structure and morphology of G-IMD. Fig. 2c presents a representative TEM image of single-layer G-IMD. The selected area electron diffraction (SAED) pattern (Fig. 2c inset) confirms the single-layer and crystalline structure because the relative intensity of {1100} spots appear to be more intense than the {2110} spots which is the characteristic of single-layer graphene.[36] In addition, by careful examination of a large number of AFM and TEM images (Fig. S3 in the ESI†), it is found that the suspension mainly contains single-layer and few-layer G-IMD and the lateral sizes are in a range of about 0.5 - 2.5 μm.

### 3.2 Dispersion of G-IMD in organic solvent and epoxy resin

Owing to the chemical functionalization, G-IMD exhibits improved compatibility with organic solvents. Fig. 3a shows the photographs of GO, rGO and G-IMD dispersion in DMF (concentration: 0.5 mg $ml^{-1}$). After storage for several weeks, the dispersion of G-IMD still remains stable while rGO forms precipitate. The good dispersibility of G-IMD makes it possible to fabricate polymer nanocomposites by commonly used solution blending technique.

To investigate the dispersion state of G-IMD in epoxy matrix, ultrathin sections of the nanocomposites with low and high content of G-IMD (0.2 and 1.5 wt %) were examined by TEM (Fig. 3b and 3c). A uniform dispersion of G-IMD thin layers, which are slightly crumpled and tortuous owing to their flexibility, is observed and no obvious aggregation occurs, further confirming that the improved organic compatibility and covalent anchoring arising from imidazole functionalization greatly promote the homogeneous dispersion of G-IMD in the epoxy matrix.

### 3.3 Catalytic effect of G-IMD

Imidazoles are commonly used as cure accelerators (or catalyst) for epoxy/anhydride systems. Though the curing reaction mechanisms are complex when accelerators are used, imidazoles are generally considered to react with the epoxide and anhydride groups, yielding active carboxylate and alkoxide anions that initiate an alternating copolymerization between epoxy and anhydride.[37] It's noteworthy that in the most of the past reports, small-molecular accelerator is commonly used and uniformly initiates the curing reaction due to its dispersion at molecular level. It's interesting that the curing reaction in this case is initiated from the interface between epoxy matrix and reinforcement, and the cure rate of epoxy monomers around G-IMD is very different from those far away.

DSC is used to evaluate the effect of G-IMD on the cure profile of the epoxy/anhydride system (Fig. 4). As shown in Fig. 4, the neat epoxy/anhydride system doesn't show obvious exothermic peak below 220 °C. With 1.0 wt % routine EMI accelerator, a sharp exothermic peak corresponding to the curing reaction appears at 123 °C. When 0.2 wt % G-IMD is added to replace EMI, an exothermic peak appears at about 160 °C. With

the increase of G-IMD content to 1.5 wt %, the peak exothermal temperature decreases to 138 °C and the peak becomes much sharper. The DSC results indicate that G-IMD can effectively catalyze the curing reaction and hence generate strong interface interaction through covalent anchoring. It is worth noting that the curing process for epoxy/anhydride systems is usually conducted between 100-200 °C. Thus fairly low contents of G-IMD are competent to replace routine accelerators for practical applications. The DSC plots for the systems with 0.4 wt % and 0.8 wt % G-IMD loading can be found in Fig. S4 and the data are summarized in Table S2 in the ESI†.

### 3.4 Tensile properties of epoxy/G-IMD nanocomposites

Representative stress-strain tensile curves of the nanocomposites and neat epoxy resin are shown in Fig. 5, and the corresponding property data, including Young's modulus, tensile strength and elongation at break are listed in Table 1. Compared with neat epoxy resin, the tensile properties of epoxy/G-IMD nanocomposites are significantly enhanced although the enhancement is non-monotonous with increasing G-IMD loading. The incorporation of 0.2 wt % and 0.4 wt % G-IMD causes 50% and 97% increase in tensile strength, 43% and 81% increase in elongation at break, 5% and 12% increase in Young's modulus, respectively. The remarkable reinforcement effects at such low G-IMD loadings can be mainly attributed to the good dispersion of G-IMD brought by its excellent organic compatibility and chemical bonding at the interface between filler and epoxy matrix.[12-14] However, with further increasing G-IMD content to 0.8 wt % and 1.5 wt %, the tensile strength and enlongation at break start to decrease, especially in case of 1.5 wt % loading. The likely reason is that excessive covalent incorporation of graphene may hinder the curing reaction between the epoxy and the curing agent, leading to a reduced crosslink density.[12,14,38] In addition, relatively high degree of functionalization and increased filler loading may cause a crowding effect during the propagation of epoxy network, and thus weaken the epoxy network locally. SEM studies provided the evidence for this, as shown below.

Fig. 6 shows representative SEM images obtained from the fracture surfaces of the epoxy/G-IMD nanocomposites and neat epoxy resin after tensile tests. The fracture surface of the neat epoxy resin is flat and smooth (Figs. 6a and 6d), indicating a brittle failure mode. In stark contrast, the fracture surfaces of the epoxy/G-IMD nanocomposites with low G-IMD loadings (0.2 wt % and 0.4 wt %) are rougher (Figs. 6b and 6e; Figs. S5a and S5c in the ESI†), signifying enhanced toughness. It can also be observed that some edge-on G-IMD sheets (white veins on the fracture surface) are homogeneously dispersed in the epoxy matrix, further confirming that almost no aggregation occurs. For the nanocomposite samples with 0.8 wt % and 1.5 wt % G-IMD, numerous micron-sized knots are observed in the SEM images (Fig. 6f; Fig S5d in the ESI†). These knots are likely to be localized dense epoxy networks, around which the networks are weaker owing to the confinement effect of graphene sheets that may restrict the crosslinking of some polymer chains. This may be an important reason that excessive G-IMD loadings would cause deterioration of mechanical properties.

For comparison purpose, an epoxy/rGO composite with 0.4 wt% rGO load was prepared as the control sample using the procedure similar to that used for the epoxy/G-IMD composites. The SEM images obtained from the fractured surface of the epoxy/rGO composite and the results of the tensile test for this sample are provided in ESI (cf. Fig S6). rGO is found to unevenly dispersed in the epoxy matrix due to its lack of functional groups, and defects caused by aggregates of rGO can also be observed. As expected, the tensile properties of the epoxy/rGO composite are distinctly poor.

### 3.5 Thermal and thermo-mechanical properties of the epoxy/G-IMD nanocomposites

To gain further insight into the interfacial interactions, the epoxy/G-IMD nanocomposites were characterized using DMA. Fig. 7 shows the storage modulus (E') and damping factor (tan δ) as a function of temperature for the neat epoxy and nanocomposites with different G-IMD loadings, and the corresponding data are summarized in Table 2. All the nanocomposite samples exhibit higher E' in glass region than the neat epoxy resin (2002 MPa). In particular, E' of the nanocomposite with 0.4 wt % G-IMD reaches the maximum value of 2403 MPa (about 20% improvement in comparison with that of neat epoxy). The significant increase in E' is mainly attributed to the good dispersion of G-IMD in the matrix and strong covalent bonds at the interface, which promotes the constrained friction and reduces the mobility of chain segments around the G-IMD.[39,40]

The peak temperature of tan δ is taken as glass transition temperature ($T_g$). As can be seen from Table 2, $T_g$ values of the epoxy/G-IMD nanocomposites display monotonic decrease, except that the $T_g$ of the sample with 0.8 wt % G-IMD is almost the same as that of neat epoxy. The decline trend may be attributed to the following two factors: (i) incorporation of short flexible alkyl chains reduces the $T_g$; (ii) G-IMD may reduce the cross-linking density of the epoxy network, leading to degradation in $T_g$.[38] Compared with neat epoxy, the tan δ peaks of the epoxy/G-IMD nanocomposites, especially the ones with 0.4 wt % and 0.8 wt % G-IMD, also become lower but broader, as shown in Fig. 7. This phenomenon is due to a broad range of relaxation temperatures in the nanocomposites as G-IMD restrains the mobility of adjacent epoxy chains through strong interface bonding and thus makes them show different relaxation behaviors with those chains far away from the interface. Similar phenomena have also been observed in other polymer-based composites reinforced by covalent incorporation of CNT or graphene.[12,14,41]

TGA is performed to investigate the thermal stabilities of the nanocomposites in a nitrogen atmosphere (Fig. 8). The data are also summarized in Table 2. All the TGA curves exhibit one main degradation stage. Compared with neat epoxy, the epoxy/G-IMD nanocomposites show higher onset degradation temperatures ($T_d$) and less weight loss in the temperature range of 300 °C to 350 °C, except the sample with 1.5 wt % G-IMD loading. The sample with 1.5 wt % G-IMD shows significantly lower $T_d$ value than the other samples because the degradation-induced active species may attack the adjacent weak chemical bonds more easily with a lower crosslink degree. The char yields of all the samples at 800 °C are proportional to the G-IMD loading because of the high thermal stability of graphene.

## Conclusions

G-IMD has been facilely prepared in one-pot though epoxy ring-opening reaction between 1-(3-Aminopropyl) imidazole and GO, followed by reduction with $NaBH_4$. The results from FTIR, XPS, TGA, XRD and elemental analysis indicate that the amino imidazole has been successfully grafted on the surface of graphene sheet. Compared with unmodified rGO, G-IMD shows enhanced organic compatibility and can be well dispersed in DMF, as well as in the epoxy resin as evidenced by the TEM and SEM images. DSC, DMA and tensile testing results reveal that G-IMD can indeed effectively catalyze the curing reaction without the addition of any routine accelerator and the tensile properties of the resultant nanocomposites are drastically enhanced at very low G-IMD loadings. Notably, the nanocomposite with 0.4 wt % G-IMD loading shows 97% increase in tensile strength and 12% increase in Young's modulus. However, excessive filler loading results in deterioration in thermal and mechanical properties as steric hindrance of graphene may cause an inhomogeneous formation of epoxy networks. In short, G-IMD can simultaneously play the roles as cure accelerator and reinforcement for the epoxy/anhydride system. The significant enhancement in mechanical properties of the epoxy/G-IMD nanocomposites mainly benefit from the improved dispersibility and interfacial covalent bonds between the G-IMD and epoxy matrix.

## Acknowledgements

This work was supported by Science and Engineering Research Council of the Agency for Science, Technology and Research (A*STAR) Singapore under Grant No. 092 137 0013.

## Notes and references

*School of Materials Science and Engineering, Nanyang Technological University, 50 Nanyang Avenue, Singapore 639798, Singapore. E-mail: asxhlu@ntu.edu.sg*

† Electronic Supplementary Information (ESI) available: [Synthesis of graphene oxide (GO), WAXS of GO, rGO and G-IMD, TGA plots of rGO and G-IMD, complementary AFM and TEM images of G-IMD; DSC of curing reaction catalysed by EMI and G-IMD; complementary SEM images from fracture surface of epoxy/G-IMD composites, SEM image from fracture surface of epoxy/rGO composites and tensile testing of pristine epoxy and epoxy/rGO composite, elemental analysis for G-IMD, DSC data of the curing reaction]. See DOI: 10.1039/b000000x/

1 R. K. Donato, L. Matejka, H. S. Schrekker, J. Plestil, A. Jigounov, J. Brus, M. Slouf, *J. Mater. Chem*., 2011, **21**, 13801.
2 K. Wang, L. Chen, J. S. Wu, M. L. Toh, C. B. He, A. F. Lee, *Macromoleculues*, 2005, **38**, 788.
3 J. H. Park, S. C. Jana, *Macromoleculues*, 2003, **36**, 2758.
4 C. S. Lim, A. J. Rodriguez, M. E. Guzman, J. D. Schaefer, *Carbon*, 2011, **49**, 1873.
5 D. R. Bortz, E. G. Heras, I. Martin-Gullon, *Macromolecules*, 2012, **45**, 238.
6 Y. Zhu, S. Murali, W. Cai, X. Li, J. W. Suk, J. R. Potts, R. S. Ruoff, *Adv. Mater*., 2010, **22**, 3906.
7 M. A. Rafiee, J. Rafiee, Z. Wang, H. Song, Z. Z. Yu, N. Koratkar, *ACS Nano*, 2009, **3**, 3884.
8 C. Lee, X. Wei, J. W. Kysar, J. Hone, *Science*, 2008, **321**, 385.
9 T. Ramanathan, A. A. Abdala, S. Stankovich, D. A. Dikin, M. Herrera-Alonso, R. D. Piner, D. H. Adamson, H. C. Schniepp, X. Chen, R. S. Ruoff, S. T. Nguyen, I. A. Aksay, R. K. Prud'homme and L. C. Brinson, *Nat. Nanotechnol*., 2008, **3**, 327.
10 X. D. Zhuang, Y. Chen, G. Liu, P. P. Li, C. X. Zhu, E. T. Kang, K. G. Neoh, B. Zhang, J. H. Zhu and Y. X. Li, *Adv. Mater*., 2010, **22**, 1731.
11 T. Kuilla, S. Bhadra, D. Yao, N. H. Kim, S. Bose, J. H. Lee, *Prog. Poly. Sci*., 2010, **35**, 1350.
12 K. S. Kim, I. Y. Jeon, S. N. Ahn, Y. D. Kwon, J. B. Baek, *J. Mater. Chem*., 2011, **21**, 7337.
13 M. Fang, Z. Zhang, J. F. Li, H. D. Zhang, H. B. Lu, Y. L. Yang, *J. Mater. Chem*., 2010, **20**, 9635.
14 C. L. Bao, Y. Q. Guo, L. Song, Y. C. Kan, X. D. Qian, Y. Hu, *J. Mater. Chem*., 2011, **21**, 13290.
15 Y. Q. Guo, C. L. Bao, L. Song, B. H. Yuan, Y. Hu, *Ind. Eng. Chem. Res*., 2011, **50**, 7772.
16 J. K. H. Teo, K. C. Teo, B. H. Pan, Y. Xiao, X. H. Lu, *Polymer*, 2007, **48**, 5671.
17 C. A. Harper, *Handbook of Plastic, Elastomers and Composites*, McGraw-Hill, New York, 1996.
18 W. S. Hummers, R. E. Offeman, *J. Am. Chem. Soc*., 1958, **80**, 1339.
19 J. K. H. Teo, C. L. Toh, X. H. Lu, *Polymer*, 2011, **52**, 1975.
20 M. Acik, G. Lee, C. Mattevi, A, Pirkle, R. M. Wallace, M. Chhowalla, K. Cho, Y. Chabal, *J. Phy. Chem. C*., 2011, **115**, 19761.
21 O. C. Compton, D. A. Dikin, K. W. Putz, L. C. Brinson, S. T. Nguyen. *Adv. Mater*., 2010, **22**, 892.
22 S. Wang, P. J. Chia, L. L. Chua, L. H. Zhao, R. Q. Png, S. Sivaramakrishnan, M. Zhou, R. G. Goh, R. H. Friend, A. T. Wee, P. K. Ho, *Adv. Mater*., 2008, **20**, 3440.
23 H. J. Shin, K. K. Kim, A. Benayad, S. M. Yoon, H. K. Park, I. S. Jung, M. H. Jin, H. K. Jeong, J. M. Kim, J. Y. Choi, Y. H. Lee, *Adv. Fuc. Mater*., 2009, **19**, 1987.
24 T. Kuila, S. Bose, P. Khanra, A. K. Mishra, N. H. Kim, J. H. Lee, *Carbon*, 2012, **50**, 914.
25 H. F. Yang, F. H. Li, C. S. Shan, D. X. Han, Q. X. Zhang, L. Niu, A. Ivaska, *J. Mater. Chem*., 2009, **19**, 4632.
26 J. Wei, P. Hing, *J. Appl. Phy*., 2002, **91**, 2812.
27 P. Zhao, L. H. Niu, L. Huang, F. S. Zhang, *J. Electrochem. Soc*., 2008, **155**, 515.
28 P. Bhunia, E. Hwang, M. Min, J. Lee, S. Seo, S. S. Some, H. Lee, *Chem. Commun*., 2012, **48**, 913.
29 G. Bhargava, T. A. Ramanarayanan, S. L. Bernasek, *Langmuir*, 2010, **26**, 215.
30 K. Idla, A. Talo, H. E. Niemi, O. Foren, S. Ylasaari, *Surf. Interface. Anal*., 1997, **25**, 837.
31 M. K. V. Bael, J. Smets, K. Schoone, L. Houben, W. McCarthy, L Adamowicz, M. J. Nowak, G. Maes, *J. Phys. Chem. A*., 1997, **101**, 2397.
32 T. J. Lane, I. Nakagawa, A. J. Kandathi, *Inorg. Chem*., 1962, **1**, 267.
33 Z. L. Wang, D. Xu, Y. Huang, Z. Wu, L. M. Wang, X. B. Zhang, *Chem. Comm*., 2012, **48**, 976.
34 S. Park, R. S. Ruoff, *Nat. Nanotechnol*., 2009, **4**, 217;
35 P. Nemes-Incze, Z. Osvath, K. Kamaras, L. P. Biro, *Carbon*, 2008, **46**, 1435.
36 Y. Hernandez, V. Nicolosi, M. Lotya, F. M. Blighe, Z. Y. Sun, S. De, I. T. Mcgovern, B. Holland, M. Byrne, Y. K. Gunko, J. J. Boland, P. Niraj, G. Duesberg, S. Krishnamurthy, R. Goodhue, J. Hutchison, V. Scardaci, A. C. Ferrari and J. N. Coleman, *Nat. Nanotechnol*., 2008, **3**, 563.
37 H. Teil, S. A. Page, V. Michaud, J. A. E. Manson, *J. Appl. Polym. Sci.*, 2004, **93**, 1774.
38 K. W. Putz, M. J. Palmeri, R. B. Cohn, R. Andrews, L. C. Brinson, *Macromolecules*, 2008, **41**, 6752.
39 P. C. Ma, S. Y. Mo, B. Z. Tang, J. K. Kim, *Carbon*, 2010, **48**, 1824.
40 T. X. Liu, I. Y. Phang, L. Shen, S. Y. Chow, W. D. Zhang, *Macromolecules*, 2004, **37**, 7214.
41 J. M. Gonzalez-Dominguez, A. M. Diez-Pascual, A. Anson-Casaos. M. A. Gomez-Fatou, M. T. Martinez, *J. Mater. Chem*., 2011, **21**, 14948.

Cite this: DOI: 10.1039/c0xx00000x

www.rsc.org/xxxxxx

**ARTICLE TYPE**

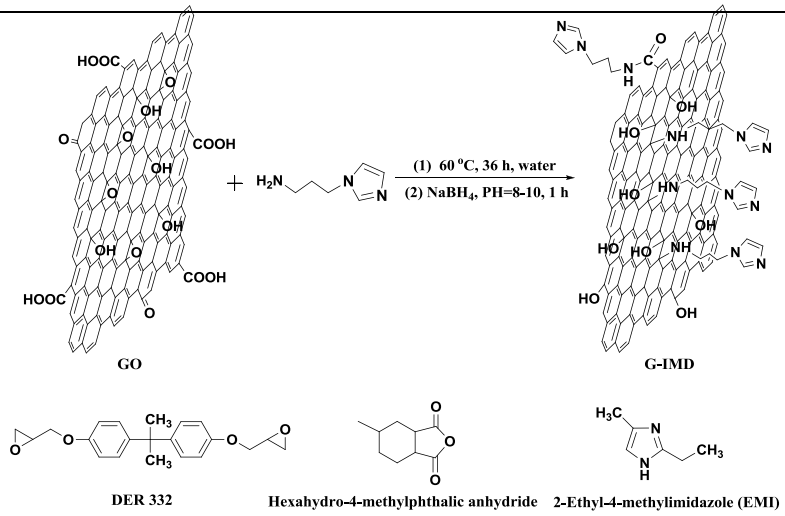


**Scheme 1** Synthesis route of G-IMD and formulas of monomers and catalyst used in this work

**Table 1** Tensile properties of the epoxy/G-IMD nanocomposites

| G-IMD Loading | Tensile Properties | | |
|---|---|---|---|
| | Young's Modulus /MPa | Tensile Strength /MPa | Elongation at Break (%) |
| 0.0 wt %[a] | 1920 ± 40 | 36 ± 3 | 2.1 ± 0.3 |
| 0.2 wt % | 2025 ± 30 | 54 ± 5 | 3.0 ± 0.2 |
| 0.4 wt % | 2140 ± 35 | 71 ± 4 | 3.8 ± 0.3 |
| 0.8 wt % | 2125 ± 60 | 45 ± 6 | 2.5 ± 0.4 |
| 1.5 wt % | 2230 ± 30 | 21 ± 3 | 0.9 ± 0.2 |

[a] Using 1 wt % EMI as cure accelerator.

**Table 2** DMA and TGA results of the epoxy/G-IMD nanocomposites

| G-IMD Loading | DMA Data | | TGA Data | |
|---|---|---|---|---|
| | Storage Modulus [b] /MPa | $T_g$ /°C | $T_d$ [c] /°C | Char Yield at 800 °C (%) |
| 0.0 wt % [a] | 2002 | 148 | 298 | 5.1 |
| 0.2 wt % | 2130 | 141 | 301 | 4.5 |
| 0.4 wt % | 2403 | 139 | 306 | 4.8 |
| 0.8 wt % | 2282 | 149 | 351 | 5.9 |
| 1.5 wt % | 2294 | 132 | 265 | 7.2 |

[a] Using 1 wt % EMI as cure accelerator. [b] Storage modulus at 50 °C.
[c] Temperature at 5% weight loss.

## Captions to Figures

**Figure 1.** C1 XPS spectra of GO, rGO and G-IMD (a); N1 XPS spectra of G-IMD (b); FTIR spectra of GO, rGO and G-IMD (c)

**Figure 2.** AFM image of G-IMD on Si wafer (a and b); TEM image of single-layer G-IMD with SAED (inset) (c).

**Figure 3.** Photograph of GO, rGO and G-IMD dispersion in DMF after several weeks (a); Representative TEM images of epoxy/G-IMD composites with 0.2 wt % (b) and 1.5 wt % (c) G-IMD loading.

**Figure 4.** DSC plots of the curing reactions catalysed by EMI and G-IMD

**Figure 5.** Stress-strain curves of pristine epoxy and epoxy/G-IMD composites (a); The average tensile strength and Young's modulus of pristine epoxy and epoxy/G-IMD composites (b).

**Figure 6.** SEM images of fracture surface obtained from tensile testing: under ×1000 magnification (a-c); under ×5000 magnification (d-f).

**Figure 7.** DMA plots of the cured epoxy/G-IMD composites

**Figure 8.** TGA plots of the cured epoxy/G-IMD composites in a nitrogen atmosphere

 

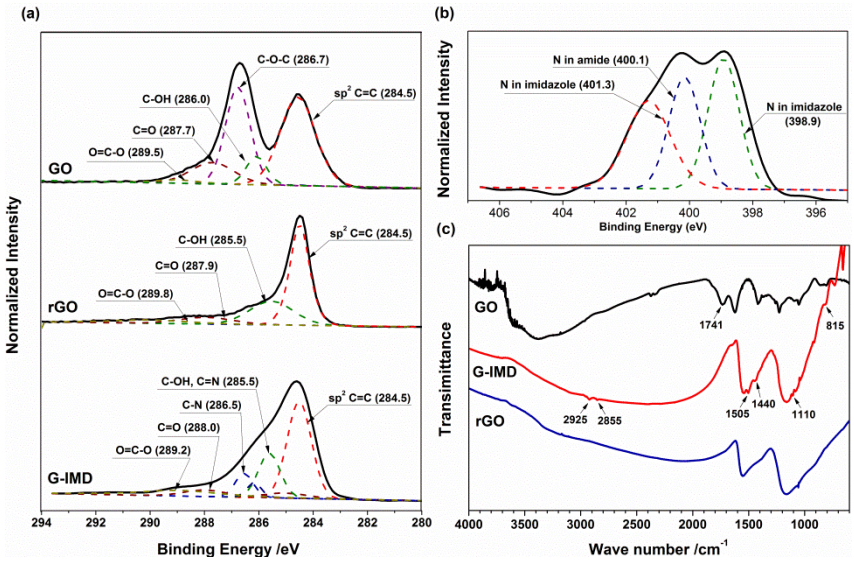


**Fig. 1** C1 XPS spectra of GO, rGO and G-IMD (a); N1 XPS spectra of G-IMD (b); FTIR spectra of GO, rGO and G-IMD (c)

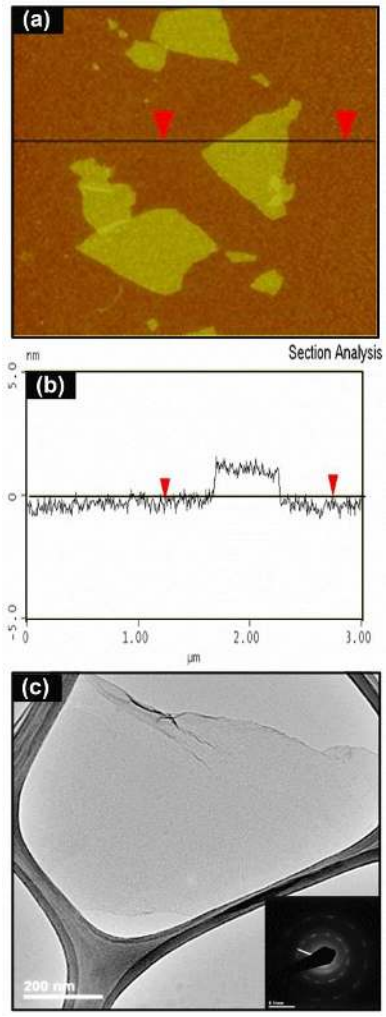


**Fig. 2** AFM image of G-IMD on Si wafer (a and b); TEM image of single-layer G-IMD with SAED (inset) (c).

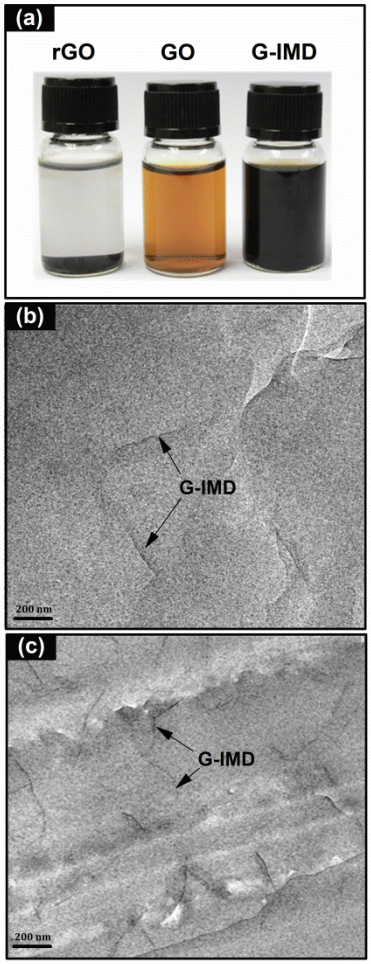


**Fig. 3** Photograph of GO, rGO and G-IMD dispersion in DMF after several weeks (a); Representative TEM images of epoxy/G-IMD composites with 0.2 wt % (b) and 1.5 wt % (c) G-IMD loading.

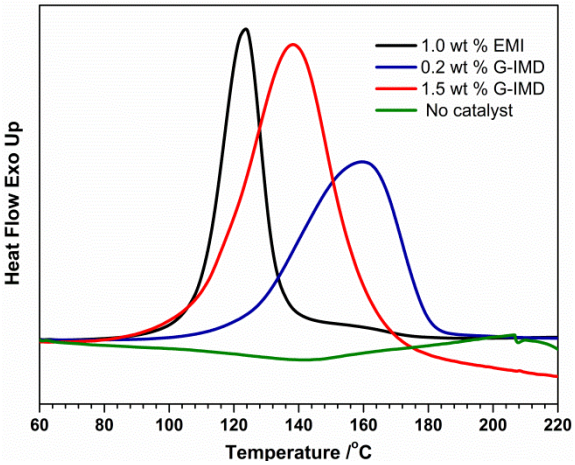


**Fig. 4** DSC plots of the curing reactions catalysed by EMI and G-IMD

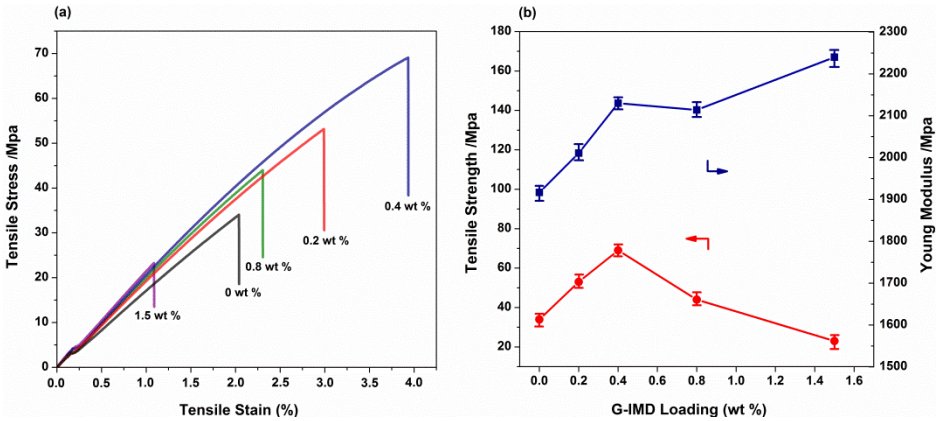


**Fig. 5** Stress-strain curves of pristine epoxy and epoxy/G-IMD composites (a); The average tensile strength and Young's modulus of pristine epoxy and epoxy/G-IMD composites (b).

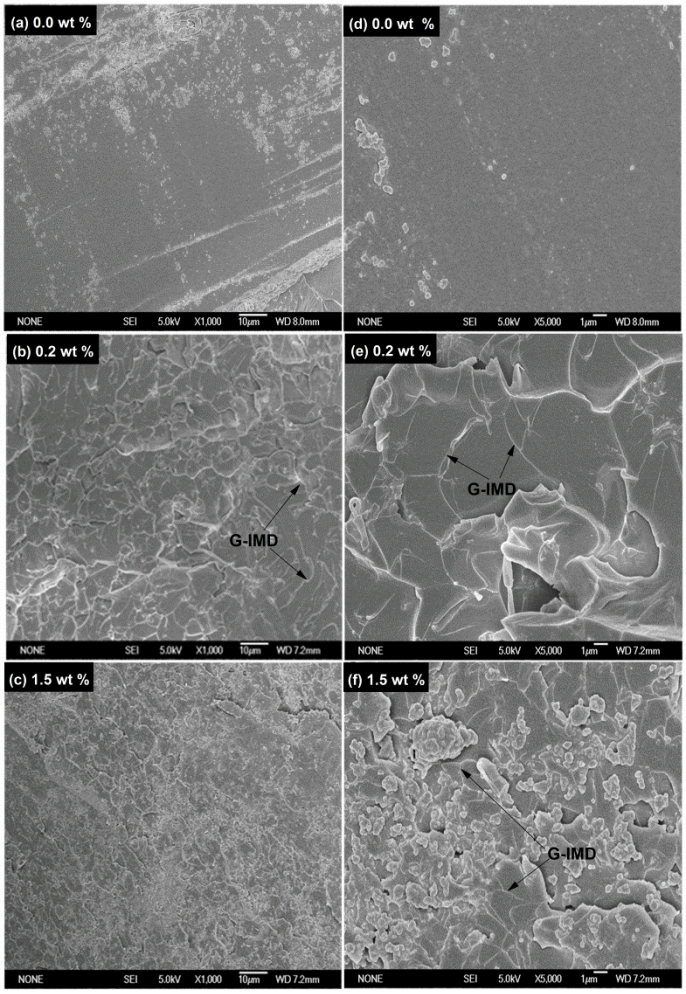


**Fig. 6** SEM images of fracture surface obtained from tensile testing: under ×1000 magnification (a-c); under ×5000 magnification (d-f).

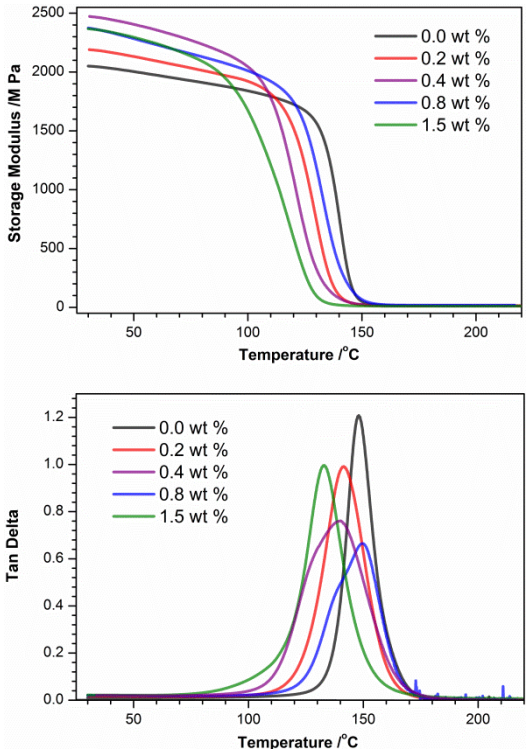


**Fig. 7** DMA plots of the cured epoxy/G-IMD composites

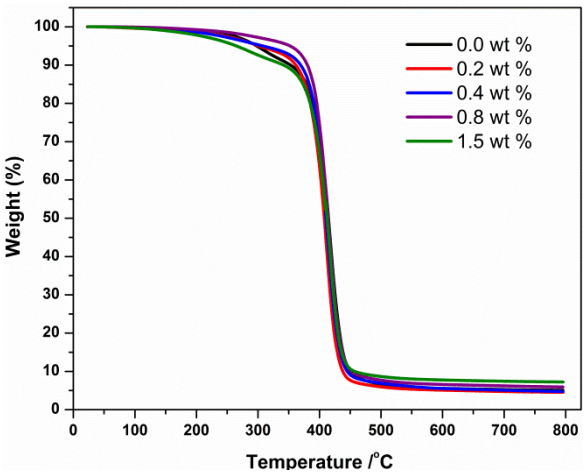


**Fig. 8** TGA plots of the cured epoxy/G-IMD composites in a nitrogen atmosphere

# Simultaneous catalyzing and reinforcing effects of imidazole-functionalized graphene in anhydride-cured epoxies†

**Wanshuang Liu, Kwang Liang Koh, Jinlin Lu, Liping Yang, Silei Phua, Junhua Kong, Zhong Chen, Xuehong Lu*.**

School of Materials Science and Engineering, Nanyang Technological University, 50 Nanyang Avenue, Singapore 639798, Singapore.(Email: asxhlu@ntu.edu.sg)

(Electronic Supplementary Information)

## Synthesis of graphene oxide (GO)

2.5 g Graphite and 2.5 g $NaNO_3$ were mixed with 120 ml sulfuric acid (95-97%) in a 500 mL flask. The mixture was stirred for 30 min in an ice bath and then 7.5 g of $KMnO_4$ was slowly added to the suspension under vigorous stirring. The ice bath was removed and the mixture was stirred at 35 $^{\circ}C$ for 24 h. Afterwards, 150 ml of deionized (DI) $H_2O$ was slowly added to the pasty mixture still under vigorous stirring. The reaction temperature was observed to rapidly increase to over 90 $^{\circ}C$ with effervescence. After 30 min, another 500 ml DI water was added, and then 1.5 mL of 30% aq. $H_2O_2$. For preliminary purification, the mixture was first washed with 5% of hydrochloric acid (HCl), followed by DI water for five times to remove residual acid and salts. The yellow mixture is centrifuged 30 min at 11,000 rpm. The obtained GO was freeze-dried for 48 h and stored in ambient environment.

 

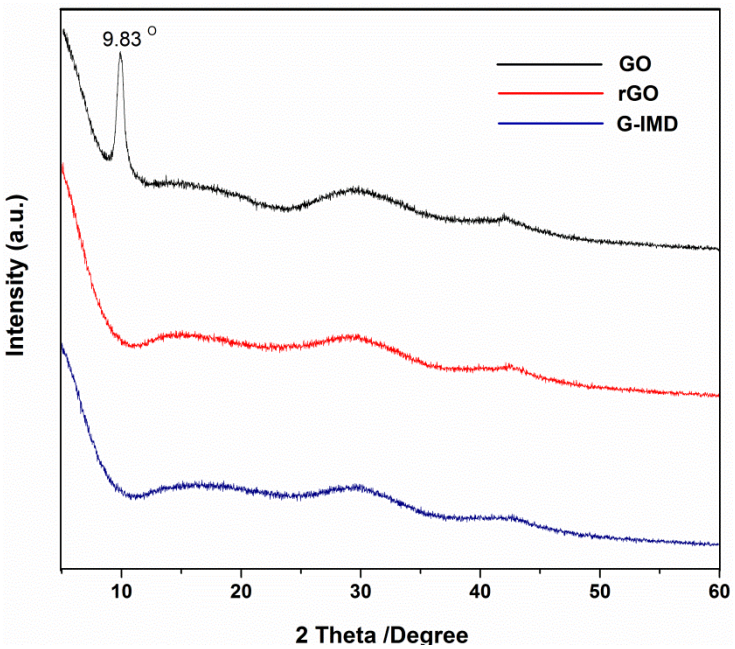


**Fig. S1** WAXS of GO, rGO and G-IMD.

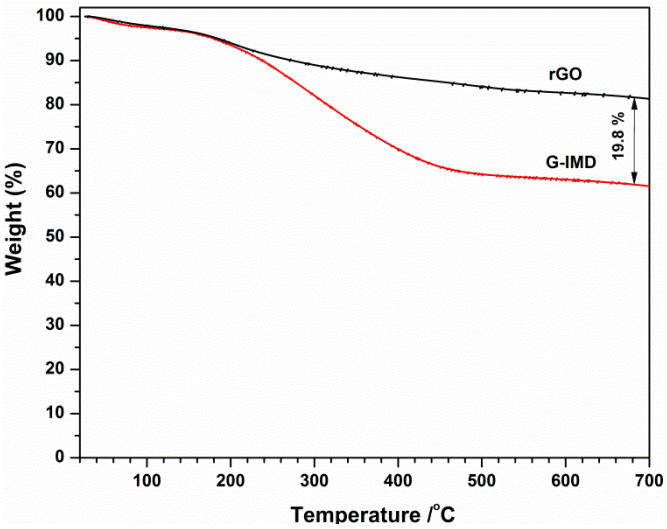


**Fig. S2** TGA plots of rGO and G-IMD in a nitrogen atmosphere.

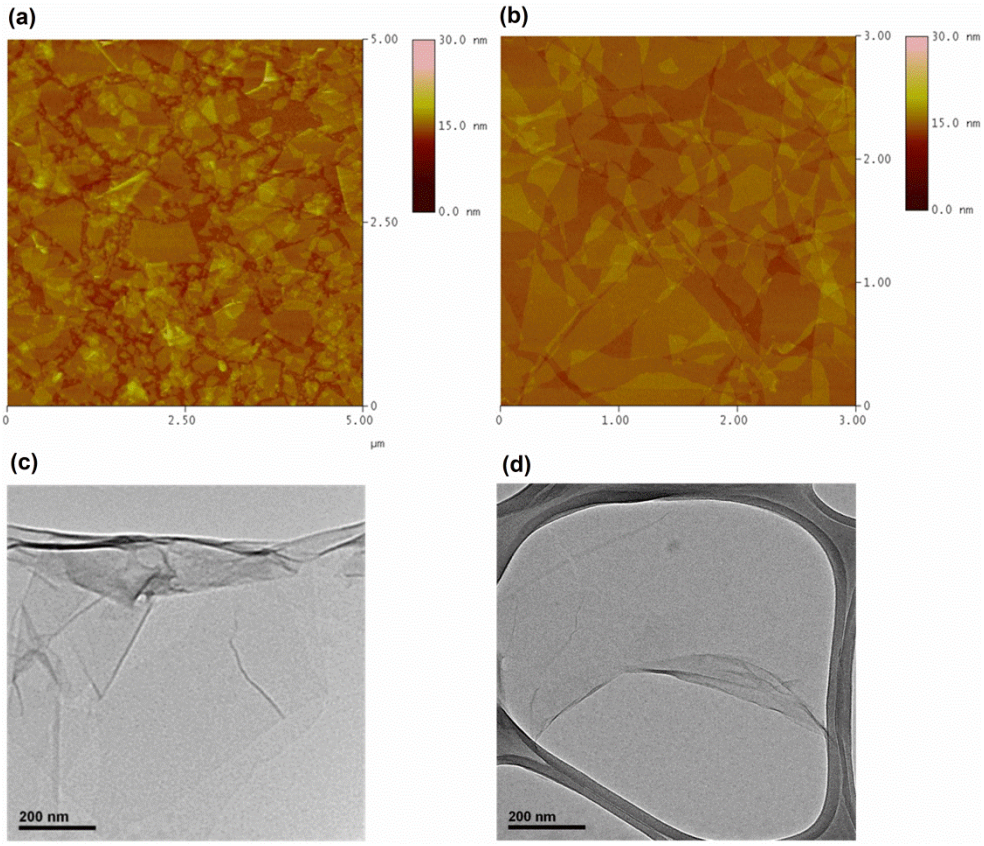


**Fig. S3** AFM (a and b) and TEM (c and d) images of G-IMD

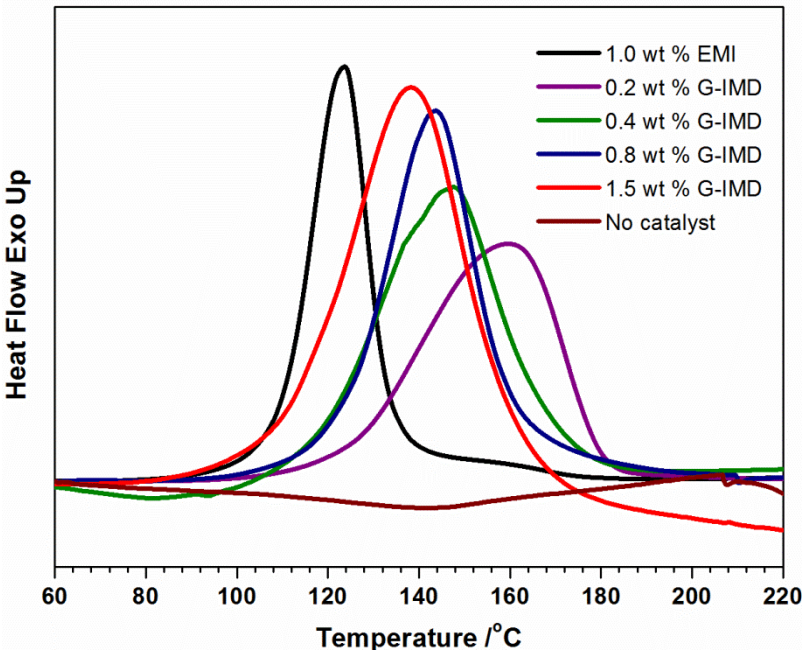


**Fig. S4** DSC plots of curing reaction catalysed by EMI and G-IMD with different filler loading.

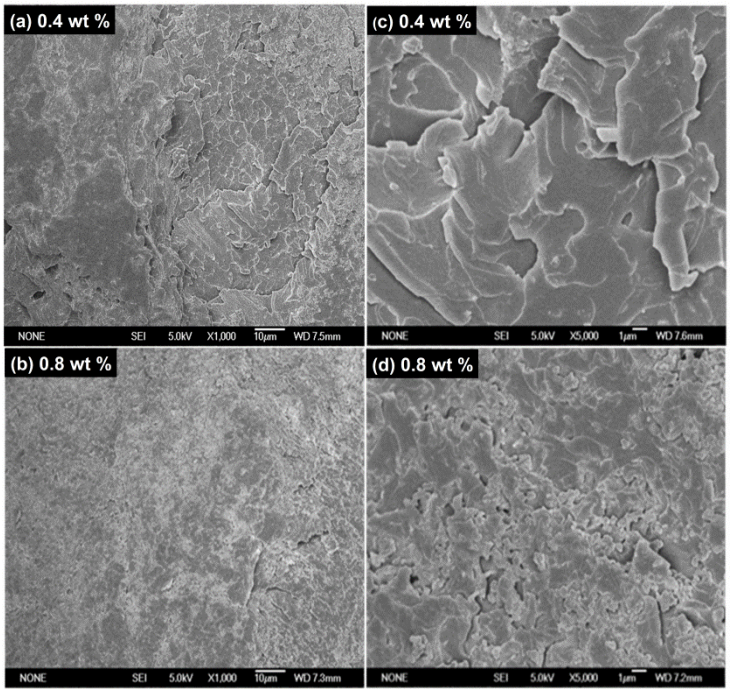


**Fig. S5** SEM images from fracture surface of epoxy/G-IMD composites after tensile testing: under ×1000 magnification (a-b); under ×5000 magnification (c-d).

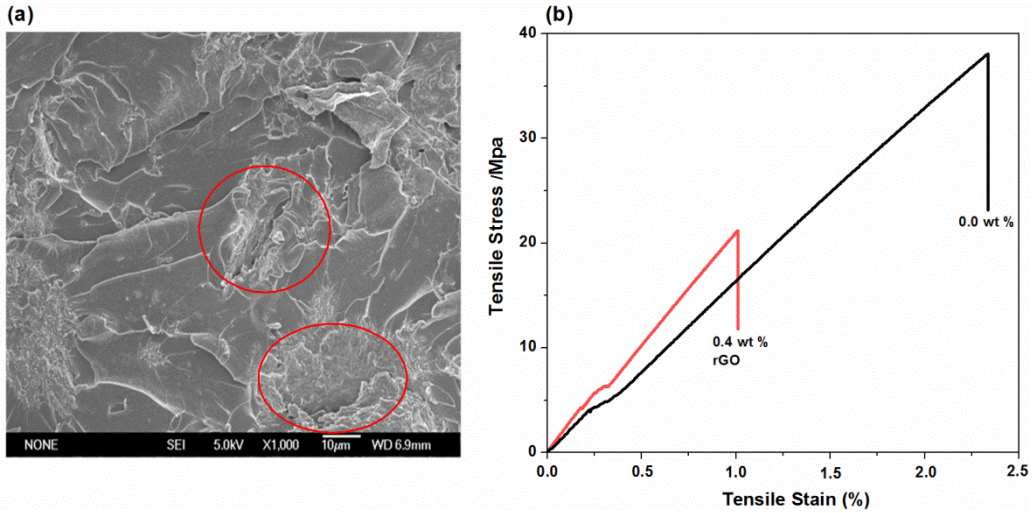


**Fig. S6** SEM image from fracture surface of epoxy/rGO composites with 0.4 wt% filler loading after tensile testing: under ×1000 magnification (a); Representative stress-strain curves of neat epoxy and epoxy/rGO composites (b).

Cite this: DOI: 10.1039/c0xx00000x

www.rsc.org/xxxxxx

ARTICLE TYPE

Table S1 Elemental analysis for G-IMD

| Element Name | Nitrogen | Hydrogen | Carbon | Difference |
|---|---|---|---|---|
| Atomic Content (wt %) | 10.92 | 4.08 | 48.48 | 36.52 |

Table S2 DSC data of the curing reaction with different accelerator content

| Catalyst content | $T_{initial}$ /°C | $T_{peak}$ /°C | $T_{end}$ /°C |
|---|---|---|---|
| Pristine Epoxy[a] | 110 | 123 | 132 |
| 0.2 wt % G-IMD | 125 | 159 | 179 |
| 0.4 wt % G-IMD | 116 | 147 | 169 |
| 0.8 wt % G-IMD | 122 | 143 | 160 |
| 1.5 wt % G-IMD | 108 | 138 | 156 |
| No catalyst | --- | --- | --- |

[a] Using 1 wt % EMI as cure accelerator

5